

Electrochemical Immunosensing of Interleukin-6 in Human Cerebrospinal Fluid and Human Serum as an Early Biomarker for Traumatic Brain Injury

Christiana Oh, Bumjun Park, Chunyan Li, Charles Maldarelli, Jennifer L. Schaefer, Timir Datta-Chaudhuri, and Paul W. Bohn*



Cite This: *ACS Meas. Sci. Au* 2021, 1, 65–73



Read Online

ACCESS |



Metrics & More



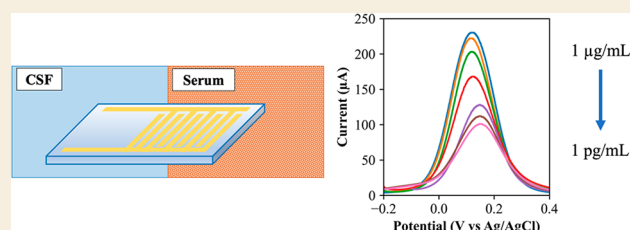
Article Recommendations



Supporting Information

ABSTRACT: In this work, we develop a label-free electrochemical immunosensor for the detection of interleukin-6 (IL-6) in human cerebrospinal fluid (CSF) and serum for diagnostic and therapeutic monitoring. The IL-6 immunosensor is fabricated from gold interdigitated electrode arrays (IDEAs) that are modified with IL-6 antibodies for direct antigen recognition and capture. A rigorous surface analysis of the sensor architecture was conducted to ensure high structural fidelity and performance. Electrochemical characterization was conducted by cyclic voltammetry (CV) and electrochemical impedance spectroscopy (EIS), and sensing was performed using differential pulse voltammetry (DPV). The DPV peak current was used to quantify IL-6 in buffer, CSF, and serum in the range $1 \text{ pg mL}^{-1} < [\text{IL-6}] < 1 \text{ } \mu\text{g mL}^{-1}$. The IL-6 IDEA sensor achieved a limit of detection (LOD) of 1.63 pg mL^{-1} in PBS, 2.34 pg mL^{-1} in human CSF, and 11.83 pg mL^{-1} in human serum. The sensor response is linear in the concentration range $10 \text{ pg mL}^{-1} < [\text{IL-6}] < 10 \text{ ng mL}^{-1}$, and the sensor is selective for IL-6 over other common cytokines, including IL-10 and TNF- α . EIS measurements showed that the resistance to charge transfer, R_{CT} , decreases upon IL-6 binding, an observation attributed to a structural change upon Ab-Ag binding that opens up the architecture so that the redox probe can more easily access the electrode surface. The IL-6 IDEA sensor can be used as a point-of-care diagnostic tool to deliver rapid results ($\sim 3 \text{ min}$) in clinical settings for traumatic brain injury, and potentially address the unmet need for effective diagnostic and prognostic tools for other cytokine-related illnesses, such as sepsis and COVID-19 induced cytokine storms. Given the interdigitated electrode form factor, it is likely that the performance of the sensor can be further improved through redox cycling.

KEYWORDS: Electrochemical sensor, biosensor, point-of-care, interdigitated electrode arrays, differential pulse voltammetry, interleukin-6, cytokines, traumatic brain injury



INTRODUCTION

With the ever-growing demand for improved diagnostic testing and health monitoring, a substantial amount of effort has been invested to identify biomolecules that can serve as indicators of physiological states, i.e., biomarkers. These efforts have led researchers to focus on cytokines, small (6–70 kDa) signaling proteins produced by cells in the immune system that regulate immune responses, inflammation, and infection trauma in complex networks.¹ Because they are pervasive in inflammation, many diseases involve cytokines, and accordingly, cytokines are widely studied as biomarkers useful to diagnosis and prognosis.^{2–4}

The sensitive quantitative determination of cytokine levels in patient samples holds great promise for early detection, leading to clinical intervention and improved patient outcomes. For example, traumatic brain injuries (TBIs) are a leading cause of death and disability in adults and children in the United States, affecting 2.5 million people every year.^{5–9} Unfortunately,

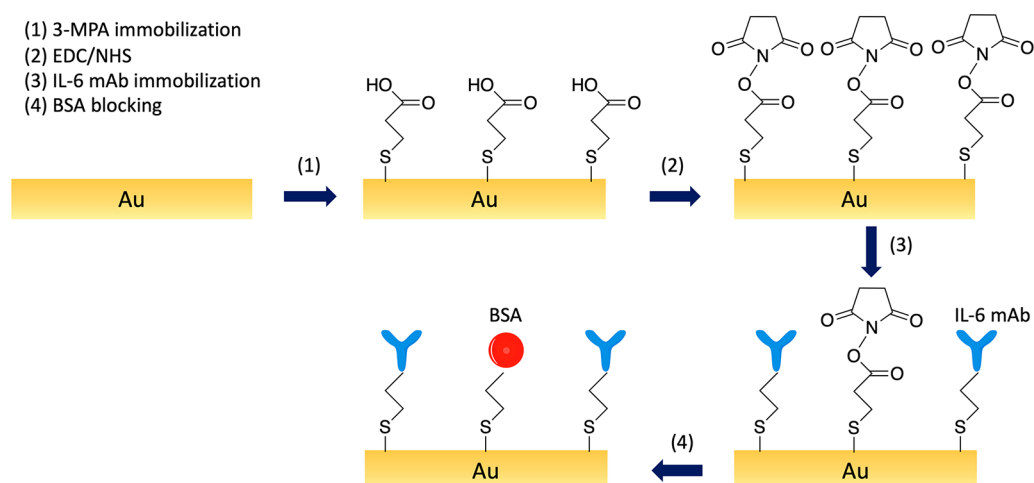
diagnosis of TBI is difficult; neurological exams to assess thinking and motor function are not definitive, and imaging tests such as CT and MRI cannot detect all TBIs. Diagnosis is further complicated by the fact that, following TBI, high levels of cytokines are released to initiate powerful inflammatory cascades that can contribute to secondary brain damage. Importantly, this post-trauma damage is a significant contributor to patient outcome and survival,^{10,11} because it is a potentially reversible pathological process.¹² Thus, the early post-traumatic monitoring of mediating cytokines takes on added importance.

Received: June 3, 2021

Published: August 9, 2021



Scheme 1. Schematic of the Au IDEA/3-MPA/IL-6 mAb/BSA Derivatization Process



Cytokines such as interleukin (IL)-1 β , IL-6, IL-8, and tumor necrosis factor-alpha (TNF- α) have been implicated in the development of inflammation following TBI. Their concentrations in both cerebrospinal fluid (CSF) and blood have been observed to rise significantly in TBI, especially during the first 24 h after injury.¹³ IL-6 is one of the most intensely studied biomarkers for TBI due to its major role in the acute phase response for inflammation in the central nervous system (CNS). Normal levels of IL-6 in the CNS are low (~ 3 pg mL⁻¹)¹⁴ but rise to as much as ~ 35 ng mL⁻¹ immediately after trauma in CSF and remain stable for several days afterward.^{10,15,16} In fact, CSF IL-6 levels have been shown to correlate with the severity of injury and survival in both children and adult TBI patients.^{17–19} Additionally, IL-6 is always found in significantly higher (≥ 10 -fold) concentrations in CSF than blood plasma or serum, although serum IL-6 levels can rise to ~ 1 ng mL⁻¹ post-TBI. Easier access to serum has dictated its predominant use in determining IL-6.^{15,20,21} Nevertheless, although the acquisition of CSF via lumbar punctures is invasive, its use is clinically recommended, and lumbar punctures are commonly performed following head injury to monitor cytokine levels and to relieve intracranial pressure post-trauma.^{22,23}

Motivated by these factors, we have developed a rapid, low-cost electrochemical immunosensor for the sensitive detection of IL-6 in human samples, such as CSF and serum, based on gold interdigitated electrode arrays (IDEAs) modified with IL-6 antibodies (IL-6 mAb) for recognition and capture of IL-6 antigen. The sensor is designed to quantify IL-6 using [Fe(CN)₆]^{3-/4-} as a redox mediator. Electrochemical sensing offers numerous advantages such as speed, sensitivity, miniaturization in a portable format, and low-cost instrumentation.^{24–27} The IL-6 IDEA sensor reported here was developed to support direct sensing, circumventing the use of labels, e.g., fluorescence, radioactivity, etc., to enable simple, straightforward detection of IL-6.

IL-6 IDEA sensor performance was assessed in buffer solution as well as whole CSF and whole serum to study the sensor's versatility and potential for use in biomedically relevant operating environments. To the authors' knowledge, this is the first report of electrochemical IL-6 sensing in whole human CSF, and we demonstrate that CSF is a desirable physiological fluid for biomarker detection. The sensor exhibits excellent sensitivity, achieving a limit of detection (LOD) of

1.63 pg mL⁻¹ in PBS and LODs of 2.34 and 11.83 pg mL⁻¹ in whole CSF and whole serum, respectively. The sensor exhibits a linear range at clinically relevant concentrations of 10 pg mL⁻¹ to 10 ng mL⁻¹ for TBI diagnosis in both CSF and serum. Preliminary experiments in buffer solution suggest that the sensitivity of the IDEA construct can be further improved by redox cycling in generator-collector (GC) mode.

Overall, these results suggest that the IL-6 IDEA sensor can be used as a point-of-care (POC) tool for diagnosis and prognosis related to TBI. Furthermore, the IL-6 IDEA sensor has potential to be used for other serious inflammation-based diseases such as sepsis, the most common cause of death in adult intensive care units,^{28–31} and COVID-19 induced cytokine storms, excessive immune responses caused by overproduction of proinflammatory cytokines, for which IL-6 is a reliable early stage biomarker.^{32–36}

EXPERIMENTAL METHODS

Reagents and Materials

3-Mercaptopropionic acid, *N*-hydroxysuccinimide (NHS), *N*-(3-(dimethylamino)propyl)-*N'*-ethylcarbodiimide hydrochloride (EDC), sulfuric acid (95–98% ACS Reagent), hydrogen peroxide 30% (w/w) solution, ethanol, 2-(*N*-morpholino)ethanesulfonic acid (MES), phosphate buffered saline (PBS, pH 7.4), monoclonal anti-interleukin-6 antibody, Tween 20, bovine serum albumin (lyophilized), potassium ferricyanide, potassium ferrocyanide, lithium perchlorate, human interleukin-6 (recombinant, expressed in *E. coli*, lyophilized), human interleukin-10 (recombinant, expressed in *E. coli*, lyophilized), and human serum (heat-inactivated, clotted from whole blood) were purchased from Millipore Sigma. IgG H&L Alexa Fluor 568 (Abcam), human TNF- α (recombinant, expressed in *E. coli*, lyophilized, PeproTech), pooled human cerebrospinal fluid (Innovative Research), and Au interdigitated electrodes on glass (10 μ m digit/gap, Metrohm Dropsens) were also used. Aqueous solutions were prepared using deionized (DI) water ($\rho = 18.2$ M Ω cm) from a Millipore Milli-Q system.

Sensor Electrode Derivatization

The derivatization procedure is shown schematically in Scheme 1. IDEAs were cleaned with piranha solution (**Caution:** piranha, 3:1 sulfuric acid/hydrogen peroxide, is a strong oxidizer and should be used with extreme caution!) for 5 min and rinsed with DI water to obtain clean hydrophilic gold surfaces. Next, IDEAs were incubated in 30 mM mercaptopropionic acid in ethanol (3-MPA) for 16 h. The resulting self-assembled monolayers (SAMs) were washed successively with ethanol and DI water. The modified electrodes were then

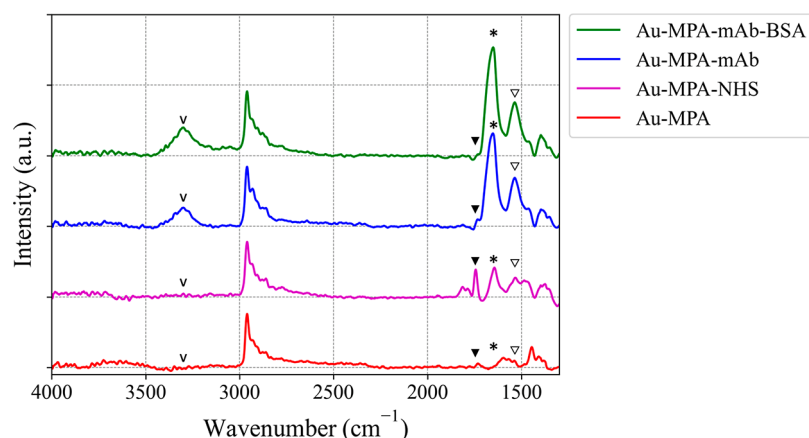


Figure 1. Grazing angle FTIR angle measurements at different steps in the immunosensor surface assembly: (1) Au-MPA, (2) Au-MPA-NHS, (3) Au-MPA-mAb, and (4) Au-MPA-mAb-BSA. Intensity values are normalized. Markers are used to indicate significant peaks of interest: 1598 cm^{-1} amide II peak (∇), 1640 cm^{-1} amide I peak (*), 1815 cm^{-1} NHS C=O stretching (\blacktriangledown), 3296 cm^{-1} N–H stretch (v).

activated with a solution of 200 mM EDC and 200 mM NHS in MES buffer (pH 5) for 1 h. IL-6 antibodies (IL-6 mAb) were covalently immobilized onto the IDEAs by incubating the electrodes in a solution 25 $\mu\text{g mL}^{-1}$ IL-6 mAb in PBS (pH 7.4) for 5 h. Electrodes were washed with 0.05% (v/v) Tween-20 solution and DI water to remove unbound antibodies and incubated in 1% (w/v) bovine serum albumin (BSA) in PBS for 1 h at 300 K to block nonspecific adsorption. After incubation in BSA solution, the electrodes were washed with 0.05% (v/v) Tween-20 and DI water to remove unbound BSA. All procedures were performed at ~ 300 K.

Grazing Angle Reflectance Fourier-Transform Infrared Spectroscopy (FT-IR)

Grazing angle reflectance FT-IR measurements were acquired on a Thermo Nicolet 6700 FTIR spectrometer with a mercury–cadmium telluride detector and a PIKE grazing angle (80°) attachment (p-polarization). These measurements were used to verify surface modification and to interrogate films between derivatization steps on one spot of a single planar Au-coated (50 nm Ti, 150 nm Au, ~ 75 mm \times 50 mm) electrode. Spectra were acquired at four points in the surface assembly process: (1) Au-MPA, (2) Au-MPA-NHS (intermediate in which $-\text{COOH}$ groups are converted to amine-reactive NHS esters), (3) Au-MPA-mAb, and (4) Au-MPA-mAb-BSA. Spectra were acquired in an N_2 atmosphere, and the background from a clean Au-coated substrate was subtracted.

Fluorescence Measurements on IL-6 IDEA Sensors

Fluorescence measurements were obtained using an Axiovert 200 M inverted fluorescence microscope and a 20x objective. To confirm IL-6 mAb immobilization on the IDEA substrates, IL-6 IDEA immunosensors were prepared using the protocol described above and incubated in a solution of 2 $\mu\text{g mL}^{-1}$ Alexa Fluor 568-conjugated 2 $^\circ$ antibody (IgG-Alexa Fluor, Abcam) in PBS (pH 7.4) for 1 h. Then they were washed with 0.05% (w/v) Tween-20 solution and DI water. The fluorescence signal produced by the IgG-Alexa Fluor was used to determine IL-6 mAb immobilization on the interdigitated electrode surface due to binding of 2 $^\circ$ IgG-Alexa Fluor to 1 $^\circ$ IL-6 mAb. Fluorescence measurements were also taken on a control IL-6 IDEA immunosensor prepared without exposure to IL-6 mAb. The control sample was then incubated in 2 $\mu\text{g mL}^{-1}$ secondary IgG-Alexa Fluor solution for 1 h and washed with 0.05% (w/v) Tween-20 solution.

Electrochemical Measurements

All cyclic voltammetry (CV) and differential pulse voltammetry (DPV) measurements were obtained on a CHI842C potentiostat (CH Instruments). Electrochemical impedance spectroscopy (EIS) measurements were taken on a PARSTAT MC1000 (Princeton Applied Research) potentiostat. Electrochemical characterization of the immunosensor assembly was performed between derivatization

steps using CV and EIS, and sensing capabilities were characterized using DPV and redox cycling CV in generator-collector mode. Electrochemical measurements were performed in 5.0 mM $\text{K}_3[\text{Fe}(\text{CN})_6]/\text{K}_4[\text{Fe}(\text{CN})_6]$ in 0.1 M LiClO_4 in PBS (pH 7.4) solution using a Pt wire counter electrode (CE) and a Ag/AgCl reference electrode (RE). For CV measurements, the potential of the working electrode (WE) was scanned from -0.4 to $+0.8$ V at a scan rate of 100 mV/s. For EIS measurements, an AC perturbation with an amplitude of 10 mV was applied at frequencies ranging from 0.1– 10^5 Hz at open circuit potential. Nyquist plots were prepared at different assembly stages by equivalent circuit fitting to a Randles circuit using a custom Python program. DPV measurements were performed at a scan rate of 0.005 V s^{-1} , pulse amplitude of 0.05 V, pulse width of 0.05 s, sample width of 0.0167 s, and pulse period of 2 s. For CV, EIS, and DPV measurements, both arms of the IDEA were biased at the same potential and used as a single working electrode enabling the sensing platform to operate in a conventional three-electrode configuration with WE, both sets Au IDEAs; CE, Pt; RE, Ag/AgCl. Generator-collector (GC) mode measurements were performed with the arms of the IDEA operated as separate working electrodes (WE1, WE2) in a four-electrode configuration. One set of IDEA digits was scanned from -0.4 to $+0.7$ V at 0.1 V s^{-1} (WE1), while the other set of digits was held at a constant potential of -0.5 V vs. Ag/AgCl (WE2).

RESULTS AND DISCUSSION

Sensor Construction and Characterization

After assembly of the immunosensor, the surface architecture was subjected to rigorous compositional and structural characterization. Grazing angle reflectance FT-IR spectra were acquired at four separate steps of the sensor surface assembly: (1) Au-MPA, (2) Au-MPA-NHS, (3) Au-MPA-mAb, and (4) Au-MPA-mAb-BSA, as shown in Figure 1. The first spectrum exhibits characteristic peaks associated with the 3-MPA SAM: OH-bending at 1444 cm^{-1} , C=O stretching at 1736 cm^{-1} , alkane C–H stretching at 2960 cm^{-1} , and OH-stretching at 3639 cm^{-1} . Upon EDC/NHS exposure, $-\text{COOH}$ groups are converted to NHS esters and new bands are observed: NHS C=O stretching at 1815 cm^{-1} , NHS ester imidyl C=O antisymmetric stretch at 1743 cm^{-1} ,³⁷ and amide I vibration at 1640 cm^{-1} .

Upon immobilization of IL-6 mAb, the spectrum shows a loss of the NHS C=O stretching peak and displays three prominent new bands indicative of protein assembly: a broad band at 3296 cm^{-1} arising from the N–H stretching of aliphatic amines, an increase in the amide I vibration peak at

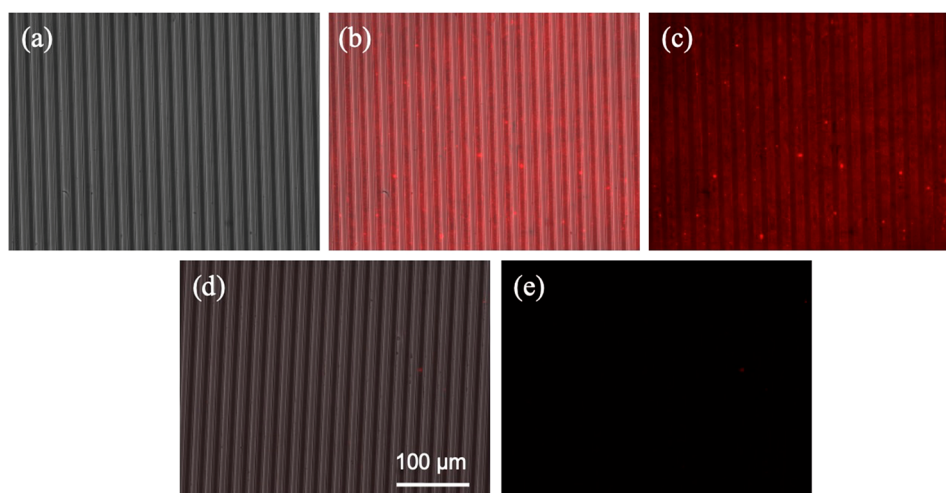


Figure 2. (a) Bright-field image of derivatized IDEA sensor. (b) Overlaid bright-field and fluorescence images of sensor after capture of IgG-Alexa Fluor 568. (c) Fluorescence image of IDEA sensor obtained by subtracting image (a) from image (b). (d) Overlaid bright-field and fluorescence images of control sensor. (e) Fluorescence image of control sensor.

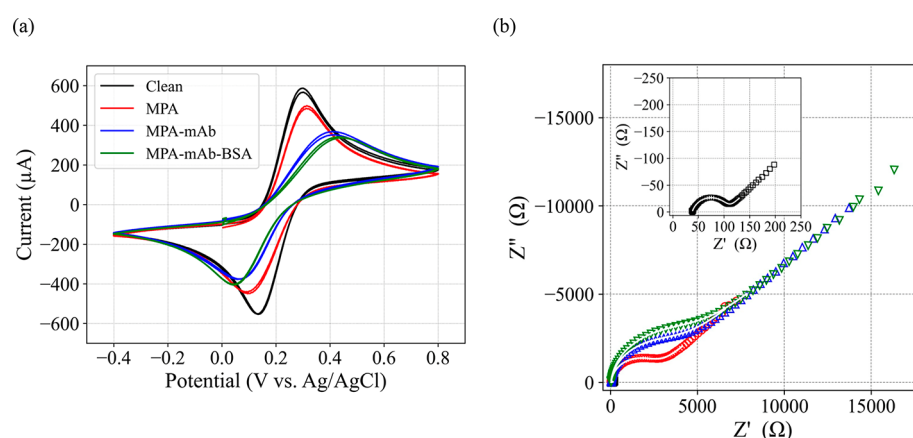


Figure 3. Electrochemical characterization of derivatized IDEA structures. (a) Cyclic voltammetry of 5 mM $\text{Fe}(\text{CN})_6^{3/4-}$ in 0.1 M LiClO_4 in PBS after each step of modification of the IL-6 IDEA immunosensor electrode. CVs were acquired at 0.1 V s^{-1} . (b) EIS spectra of 5 mM $\text{Fe}(\text{CN})_6^{3/4-}$ in 0.1 M LiClO_4 in PBS after each step of modification of the IL-6 IDEA immunosensor electrode. Inset: Underivatized (clean) electrode. Color scheme in the main figure identical to that in panel (a). Fitted EIS response curves shown as solid white lines.

1640 cm^{-1} , and an amide II peak at 1598 cm^{-1} . The final spectrum indicates immobilization of BSA blocking protein based on the increase in absorbance for the characteristic protein peaks. The FT-IR spectra acquired at sequential steps of immobilization of the Au substrate confirm successful functionalization. Furthermore, these results are supported by contact angle measurements taken in parallel with the FT-IR measurements (Figure S1, Supporting Information, SI).

After validating the immobilization of IL-6 mAb on planar Au-coated substrates, the procedure was applied to the Au IDEA digits to prepare IL-6 IDEA immunosensors. Completely functionalized IDEA sensors were incubated in $2 \mu\text{g mL}^{-1}$ 2° IgG-Alexa Fluor 568 solution to allow for 1° IL-6 mAb- 2° IgG-Alexa Fluor binding. Bright-field and fluorescence images were obtained, Figure 2a–c, and the resulting background-subtracted fluorescence-only image, Figure 2c, confirmed successful, selective immobilization of primary IL-6 mAb on the electrode digits. Bright-field and fluorescence images obtained for a control IDEA sensor prepared without immobilization of 1° IL-6 mAb and incubated in identical 2° IgG-Alexa Fluor solution, Figure 2d and e, indicated no

fluorescence signal in the absence of the IL-6 mAb. Although there is a small amount of spatial heterogeneity in the fluorescence on the derivatized digits, these results clearly show that the fluorescence signal resulted from 1° IL-6 mAb- 2° IgG-Alexa Fluor binding, rather than physical adsorption of the 2° IgG-Alexa Fluor directly onto the electrode. Thus, the fluorescence images of the IL-6 IDEA sensor demonstrate uniform IL-6 mAb immobilization on the IDEA surfaces, confirming the high structural fidelity of the IL-6 sensing interface.

The immunosensor assembly was also characterized after each derivatization step using CV and EIS, as shown in Figure 3a. A well-behaved pair of redox peaks was observed in the cyclic voltammograms for the underivatized IDEA. However, as additional layers were functionalized on the electrode, significant changes in the cyclic voltammograms were observed: (i) decreases in the current, suggesting a reduction in the effective electroactive surface area, and (ii) greater peak separation, indicating more sluggish kinetics with increasing derivatization. The data were further used in conjunction with the Randles–Sevcik equation to estimate the electroactive area

Table 1. Randles Circuit Component Values of the IL-6 immunosensor

	R_s (Ω) ^a	R_{CT} (Ω)	σ ($\Omega/s^{1/2}$)	χ^2
Au	39.7 ± 1.1	65.2 ± 1.3	73.8 ± 0.7	8.96 × 10 ⁻⁵
Au-MPA	30.7 ± 1.4	2559.7 ± 9.7	4020.5 ± 21.0	5.37 × 10 ⁻⁴
Au-MPA-mAb	33.0 ± 1.0	3860.1 ± 10.1	8164.0 ± 13.4	3.37 × 10 ⁻⁴
Au-MPA-mAb-BSA	30.1 ± 1.1	4699.8 ± 12.1	9795.9 ± 14.8	5.63 × 10 ⁻⁴

^aQuoted parameter errors indicate standard errors.

(Table S1), which was found to decrease at every step in the derivatization.

EIS measurements were also used to electrochemically characterize the derivatization process, as shown in Figure 3b. The experimental data were fitted to a standard Randles circuit to generate Nyquist plots for the IDEA substrate at each derivatization stage. Based on the fitting to a Randles model circuit,³⁸ the values for circuit components were obtained at each derivatization stage, and the χ^2 goodness-of-fit parameters were calculated, Table 1. A Nyquist plot for the underivatized sensor substrate is shown in the inset of Figure 3b, which after assembly of the 3-MPA SAM shows clear indications of the formation of a kinetic barrier to electron transfer of $[\text{Fe}(\text{CN})_6]^{3/4-}$, consistent with the increased charge transfer resistance, R_{CT} , recovered from the model, Table 1. Addition of the IL-6 mAb and BSA blocking protein layers were accompanied by further increases in R_{CT} , with the Warburg coefficient, σ , providing additional evidence of an increasing kinetic barrier to electron transfer as the electrode is progressively functionalized.

Electrochemical Sensing of IL-6 in PBS

Initial experiments to assess sensor response to the change in interfacial properties of the IL-6 IDEA electrodes due to Ab-Ag binding were conducted via EIS. IL-6 IDEA immunosensors were incubated in 1 ng mL⁻¹ IL-6 standard solutions for 20 min, followed by washing and immediate measurement. Typical results are shown in Figure 4 and Table 2. Surprisingly,

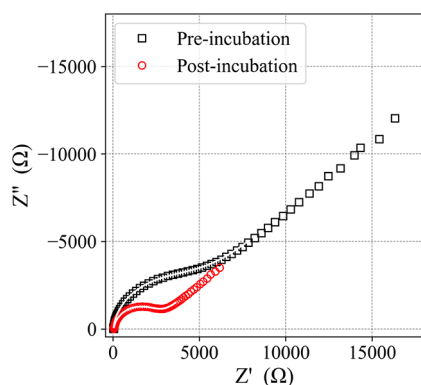


Figure 4. Nyquist plots from IL-6 IDEA sensors before and after exposure to 1 ng mL⁻¹ IL-6 in 0.1 M LiClO₄ in PBS. Fitted curves were added as solid white lines.

R_{CT} decreases upon incubation with the analyte, an unexpected result. Surface characterization by the spectroscopic and electrochemical techniques presented above confirm the covalent immobilization of IL-6 antibodies and sensor stabilization by BSA blocking proteins. Ellipsometry measurements (SI) also support the formation of a well-structured and functional IL-6 mAb/Ag binding layer based on the increase in surface film thickness after incubation of the immunosensor with IL-6 (Table S2).

Similar EIS results have been reported³⁹ in which a decrease in R_{CT} was observed upon IL-6 Ab-Ag binding on a gold microelectrode array. The authors attributed this to a characteristic of the microelectrode architecture used in their study. In addition, other biosensing studies that utilize $\text{Fe}(\text{CN})_6^{3/4-}$ as the redox probe have reported analogous unexpected EIS results and even utilized reduction in R_{CT} upon target binding as a sensing principle.^{40–44} While these studies have attributed the reduction of R_{CT} upon antigen binding to a number of disparate factors, we hypothesize that the most likely explanation is a structural change upon Ab-Ag binding that opens up the architecture so that the redox probe can more easily access the electrode surface.

After establishing proper sensor assembly and function, IL-6 IDEA sensors were incubated in IL-6 in PBS (pH 7.4) solutions at concentrations ranging from 1 pg mL⁻¹ to 1 μg mL⁻¹ for 30 min at 300 K. After incubation, the sensors were washed extensively with 0.05% (w/v) Tween-20 solution and DI water to remove unbound species. Next, DPV measurements were acquired immediately in 5.0 mM $\text{Fe}(\text{CN})_6^{3/4-}$, 0.1 M LiClO₄ in PBS. At each IL-6 concentration, the DPV response was averaged over 5 individual sensors, Figure 5a. The effect of IL-6 concentration on the peak current, I_p , was evaluated and used to generate a calibration curve, Figure 5b. I_p decreases with increasing IL-6 analyte concentration, suggesting increasing passivation of the electrode due to IL-6 antibody capture by the immobilized IL-6 mAb. The DPV peaks shift slightly, from ~+0.10 to +0.15 V with increasing IL-6 concentrations, Figure 5a, a phenomenon commonly observed in DPV-based electrochemical biosensing, which is attributed to hindered transport of redox probe to the electrode/electrolyte interface with increased Ab-Ag binding. The I_p working curve in Figure 5b is sigmoidal, as expected, with a linear response to the log of the IL-6 analyte concentration from ca. 10 pg mL⁻¹ to 10 ng mL⁻¹ and a LOD of 1.63 pg mL⁻¹ in PBS buffer.

Table 2. Randles Circuit Component Values of IL-6 Immunosenor Pre- and Postincubation

	R_s (Ω) ^a	R_{CT} (Ω)	σ ($\Omega/s^{1/2}$)	χ^2
preincubation	30.1 ± 1.1	4699.8 ± 12.1	9795.9 ± 14.8	5.63 × 10 ⁻⁴
postincubation	38.8 ± 1.1	2516.3 ± 6.5	2930.5 ± 14.0	2.17 × 10 ⁻³

^aQuoted parameter errors indicate standard errors.

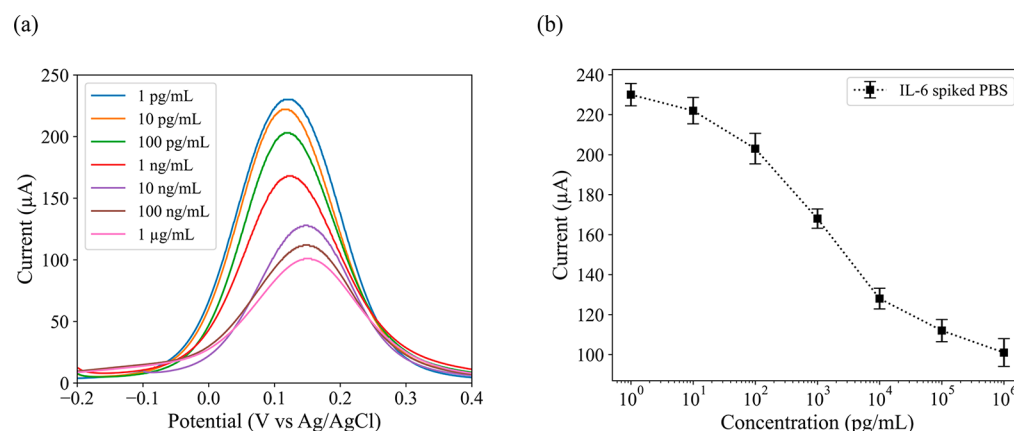


Figure 5. Performance of the IL-6 electrochemical immunosensor. (a) DPV current response as a function of IL-6 concentration in the range 1 pg mL⁻¹ to 1 μg mL⁻¹. (b) Working curve based on DPV I_p values. Errors represent ± 1 standard deviation measured across $n = 5$ different sensors at each concentration.

Sensor Selectivity

TNF- α and IL-10 were selected as model interferences to challenge the selectivity of the IL-6 sensor due to their presence in CSF and serum following TBI. TNF- α is also a proinflammatory cytokine whose levels elevate in the early stages post-TBI, while IL-10 is an anti-inflammatory cytokine whose levels rise rapidly and stabilize hours after TBI. To test sensor selectivity, IL-6 IDEA sensors were challenged individually with the nontarget cytokine (TNF- α , or IL-10) at concentrations in the range 100 pg mL⁻¹ to 100 ng mL⁻¹ in PBS. DPV measurements were acquired under the same conditions used for IL-6, except TNF- α and IL-10 DPV results were averaged over 3 sensor devices. The results compared against the DPV response for IL-6 in Figure 6 show that when

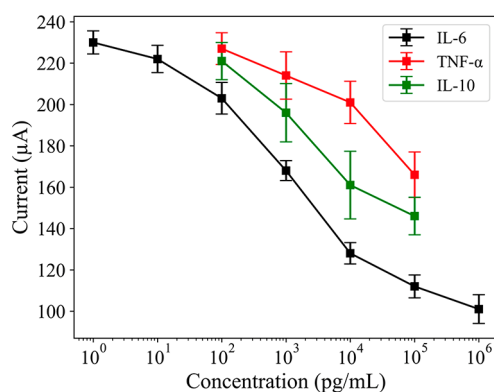


Figure 6. DPV working curves for TNF- α (red), IL-10 (green), and IL-6 (black) standard solutions in PBS. Errors for TNF- α and IL-10 represent ± 1 standard deviation across $n = 3$ sensor devices.

IL-6 IDEA sensors are challenged against TNF- α or IL-10, the I_p values are significantly higher than those for IL-6 at the same concentration. Another way to interpret the plot is assess the concentration change needed to cause the same normalized ΔI_p . Examined according to this criterion, the sensor exhibits ca. 10 \times selectivity for IL-6 over IL-10 and ca. 100 \times selectivity over TNF- α . Thus, the IL-6 IDEA sensor is specific for the target analyte and exhibits good resistance toward nonspecific binding.

Sensing in Human Cerebrospinal Fluid and Serum

To validate the sensor for clinical applications, the IL-6 IDEA sensors were tested in human-derived cerebrospinal fluid (CSF) and serum. Assays and measurements were undertaken with the same methods that were used for PBS-based DPV experiments. Standard solutions were prepared from both types of physiological samples in the range 1 pg mL⁻¹ to 1 μg mL⁻¹, and DPV I_p values obtained from five individual sensors at each IL-6 concentration were used to generate the working curves for CSF (blue) and serum (red), as shown in Figure 7.

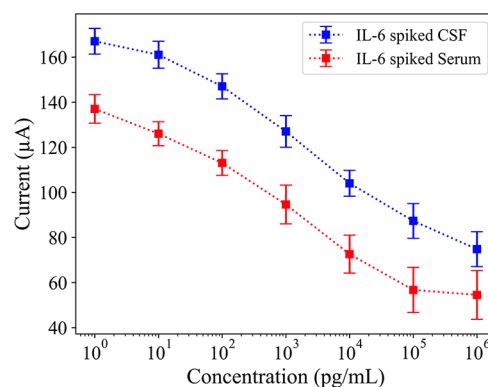


Figure 7. Sensor performance with human-derived samples. IL-6 IDEA sensor working curves for IL-6 spiked in human CSF (blue) and human serum (red). Error bars represent ± 1 standard deviation across $n = 5$ sensors at each concentration.

Both working curves follow similar sigmoidal trends, and in whole CSF the sensor shows a linear sensing range of 10 pg mL⁻¹ to 10 ng mL⁻¹ and a LOD of 2.34 pg mL⁻¹, while in serum the sensor shows the same linear range and a LOD of 11.83 pg mL⁻¹. The superior performance of the immunosensor in CSF is attributed to the lower background of potential interferences in CSF relative to serum.

The performance of the IL-6 IDEA sensor was also explored in both CSF and serum. The IDEA sensor is less sensitive to IL-6 in CSF and serum than in PBS, which is expected due to the presence of interferences, such as cellular debris, proteins, lipids, etc. In addition, the LOD was higher by a factor of approximately 1.5 in CSF compared to PBS, while the corresponding LOD in serum was an order of magnitude

higher. The larger LOD in serum than in CSF is likely due to the higher serum protein content; typically, total CSF protein (15 to 60 mg dL⁻¹) is ~1% of total serum protein (6–8 g dL⁻¹).

CONCLUSIONS

A highly sensitive, label-free immunosensing platform based on Au IDEAs was developed for the detection of IL-6, a critical cytokine biomarker for inflammation and trauma. In comparing the performance of the IL-6 IDEA sensor to other biosensors, it exhibits a LOD in PBS that is comparable to other label-free sensors and ELISA-based electrochemical immunosensors, and it achieves linear ranges at IL-6 concentrations across 4 orders of magnitude for all fluids, which is wider than that of most label-free electrochemical immunosensors. Thus, the IL-6 IDEA sensor is an excellent candidate for clinical application as a POC tool, given its simple assembly, ease of operation, straightforward analysis, and good sensitivity for IL-6 in physiological fluids. Furthermore, it may be possible to extend the sensitivity. Preliminary experiments on nonoptimized structures show that the IDEAs can operate in generator-collector redox cycling mode and produce amplification factors of 3–5 (SI). We expect further development of these architectures to yield comparably lower LODs. Additionally, the IL-6 IDEA electrochemical immunosensor can reliably detect IL-6 across 4 orders of magnitude at clinically relevant concentrations in CSF and serum. Thus, CSF is a desirable physiological fluid for biomarker detection due to its exceptionally low concentration of nontarget interferents relative to blood plasma or serum.

Overall, the IL-6 IDEA sensor is a versatile, low-cost POC diagnostic tool that can deliver rapid (~3 min) results for traumatic brain injury and also address the unmet need for effective diagnostic and prognostic tools for other cytokine-related illnesses, such as sepsis, a systemic inflammatory response that takes nearly 270 000 American lives per year.⁴⁵ A significant factor associated with the high mortality rate in sepsis patients is delayed diagnosis, caused by nonspecific initial symptoms and a lack of rapid diagnostic tools for sepsis. Blood cultures, the clinical gold standard in diagnosing sepsis, take 2–3 days to return results. Early detection, which can potentially be achieved through the sensitive detection of inflammatory cytokines, and timely administration of antibiotics are the two most important factors in improving sepsis patient outcome.⁴⁶ Another example of dangerous hyper-inflammatory responses is “cytokine storms” which are gaining increased attention due to their association with the most severe cases of COVID-19 and are implicated in 20–30% of all COVID-19 deaths. Because the runaway immune response rapidly escalates to severe medical complications and eventually death, treatment requires early detection and intervention. Recent studies suggest that elevated levels of IL-6 are a reliable precursor to COVID-19 cytokine storms as well as adverse patient outcomes, e.g., intensive care unit admission, severe medical complications, acute respiratory distress syndrome, and death.^{47–50} The electrochemical immunosensor developed here has the potential to be an effective tool to address the unmet clinical need for near-real time and ultrasensitive tools for deadly inflammation-based diseases and illnesses.

ASSOCIATED CONTENT

Supporting Information

The Supporting Information is available free of charge at <https://pubs.acs.org/doi/10.1021/acsmeasuresciau.1c00013>.

Contact angle measurements, electroactive area calculations, ellipsometry measurements, and generator-collector mode redox cycling experiments (PDF)

AUTHOR INFORMATION

Corresponding Author

Paul W. Bohn – Department of Chemical and Biomolecular Engineering and Department of Chemistry and Biochemistry, University of Notre Dame, Notre Dame, Indiana 46556, United States; orcid.org/0000-0001-9052-0349; Email: pbohn@nd.edu

Authors

Christiana Oh – Department of Chemical and Biomolecular Engineering, University of Notre Dame, Notre Dame, Indiana 46556, United States; orcid.org/0000-0002-6018-920X

Bumjun Park – Department of Chemical and Biomolecular Engineering, University of Notre Dame, Notre Dame, Indiana 46556, United States; orcid.org/0000-0002-3779-1315

Chunyan Li – Institute for Bioelectronic Medicine, Feinstein Institutes for Medical Research, Manhasset, New York 11030, United States

Charles Maldarelli – The Benjamin Levich Institute for Physicochemical Hydrodynamics and Department of Chemical Engineering, The City College of New York, New York, New York 10031, United States; orcid.org/0000-0001-7427-2349

Jennifer L. Schaefer – Department of Chemical and Biomolecular Engineering, University of Notre Dame, Notre Dame, Indiana 46556, United States; orcid.org/0000-0003-4293-6328

Timir Datta-Chaudhuri – Institute for Bioelectronic Medicine, Feinstein Institutes for Medical Research, Manhasset, New York 11030, United States; orcid.org/0000-0001-7377-1939

Complete contact information is available at: <https://pubs.acs.org/10.1021/acsmeasuresciau.1c00013>

Notes

The authors declare no competing financial interest.

ACKNOWLEDGMENTS

This work was supported by the National Science Foundation through an Intern supplement IIP1404744 and through Grant CHE1904196. C.O. was also partially supported by a Berry Family Fellowship through Notre Dame's Institute for Precision Health. The authors are grateful to M. Bruening and L. Yang for assistance with FTIR and ellipsometry measurements as well as guidance on experiments with biological fluids. The authors are also grateful for useful discussions with J. Berwanger, H. Zhou, and A. Chan on various aspects of the experiments.

REFERENCES

(1) Stenken, J. A.; Poschenrieder, A. J. Bioanalytical Chemistry of Cytokines - A Review. *Anal. Chim. Acta* **2015**, 853 (1), 95–115.

- (2) Goldys, E. M.; Liu, G.; Qi, M.; Hutchinson, M. R.; Yang, G. Recent Advances in Cytokine Detection by Immunosensing. *Biosens. Bioelectron.* **2016**, *79*, 810–821.
- (3) Doll, D. N.; Barr, T. L.; Simpkins, J. W. Cytokines: Their Role in Stroke and Potential Use as Biomarkers and Therapeutic Targets. *Aging Dis.* **2014**, *5* (5), 294–306.
- (4) Oppenheim, J. J.; Rossio, J. L.; Gearing, A. J. H. *Clinical Applications of Cytokines: Role in Pathogenesis, Diagnosis, and Therapy*; Oxford University Press, 1993.
- (5) Centers for Disease Control. Incidence Rates of Hospitalization Related to Traumatic Brain Injury—12 States, 2002. *MMWR Morb. Mortal. Wkly. Rep.* **2006**, *55* (8), 201–204.
- (6) Adekoya, N.; Thurman, D. J.; Webb, K. W.; White, D. D. *Surveillance for Traumatic Brain Injury Deaths -- Centers for Disease Control and Prevention, 1989–1998*.
- (7) Coronado, V. G.; Xu, L.; Basavaraju, S. V.; McGuire, L. C.; Wald, M. M.; Faul, M.; Hemphill, J. D. *Surveillance for Traumatic Brain Injury-Related Deaths*; U.S. Dept. of Health and Human Services, Centers for Disease Control and Prevention, 1997–2007.
- (8) Vella, M. A.; Crandall, M. L.; Patel, M. B. Acute Management of Traumatic Brain Injury. *Surg. Clin. North Am.* **2017**, *97* (5), 1015–1030.
- (9) Khellaf, A.; Khan, D. Z.; Helmy, A. Recent Advances in Traumatic Brain Injury. *J. Neurol.* **2019**, *266* (11), 2878–2889.
- (10) Morganti-Kossmann, M. C.; Lenzlinger, P. M.; Hans, V.; Stahel, P.; Csuka, E.; Ammann, E.; Stocker, R.; Trentz, O.; Kossmann, T. Production of Cytokines Following Brain Injury: Beneficial and Deleterious for the Damaged Tissue. *Mol. Psychiatry* **1997**, *2* (2), 133–136.
- (11) Povlishock, J. T.; Christman, C. W. The Pathobiology of Traumatically Induced Axonal Injury in Animals and Humans: A Review of Current Thoughts. *J. Neurotrauma* **1995**, *12* (4), 555–564.
- (12) Arand, M.; Melzner, H.; Kinzl, L.; Brückner, U.; Gebhard, F. Early Inflammatory Mediator Response Following Isolated Traumatic Brain Injury and Other Major Trauma in Humans. *Langenbeck's Arch. Surg.* **2001**, *386* (4), 241–248.
- (13) Maier, B.; Schwerdtfeger, K.; Mautes, A.; Holanda, M.; Müller, M.; Steudel, W. I.; Marzi, I. Differential Release of Interleukines 6, 8, and 10 in Cerebrospinal Fluid and Plasma after Traumatic Brain Injury. *Shock* **2001**, *15* (6), 421–426.
- (14) Schwieler, L.; Larsson, M. K.; Skogh, E.; Kegel, M. E.; Orhan, F.; Abdelmoaty, S.; Finn, A.; Bhat, M.; Samuelsson, M.; Lundberg, K.; Dahl, M.-L.; Sellgren, C.; Schuppe-Koistinen, I.; Svensson, C.; Erhardt, S.; Engberg, G. Increased Levels of IL-6 in the Cerebrospinal Fluid of Patients with Chronic Schizophrenia—Significance for Activation of the Kynurenine Pathway. *J. Psychiatry Neurosci.* **2015**, *40* (2), 126–133.
- (15) Hayakata, T.; Shiozaki, T.; Tasaki, O.; Ikegawa, H.; Inoue, Y.; Toshiyuki, F.; Hosotubo, H.; Kieko, F.; Yamashita, T.; Tanaka, H.; Shimazu, T.; Sugimoto, H. Changes in CSF S100B and Cytokine Concentrations in Early-Phase Severe Traumatic Brain Injury. *Shock* **2004**, *22* (2), 102–107.
- (16) Kumar, R. G.; Diamond, M. L.; Boles, J. A.; Berger, R. P.; Tisherman, S. A.; Kochanek, P. M.; Wagner, A. K. Acute CSF Interleukin-6 Trajectories after TBI: Associations with Neuroinflammation, Polytrauma, and Outcome. *Brain, Behav., Immun.* **2015**, *45*, 253–262.
- (17) Woiciechowsky, C.; Schöning, B.; Cobanov, J.; Lanksch, W. R.; Volk, H.-D.; Döcke, W.-D. Early IL-6 Plasma Concentrations Correlate with Severity of Brain Injury and Pneumonia in Brain-Injured Patients. *J. Trauma* **2002**, *52* (2), 339–345.
- (18) Singhal, A.; Baker, A. J.; Hare, G. M. T.; Reinders, F. X.; Schlichter, L. C.; Moulton, R. J. Association between Cerebrospinal Fluid Interleukin-6 Concentrations and Outcome after Severe Human Traumatic Brain Injury. *J. Neurotrauma* **2002**, *19* (8), 929–937.
- (19) Bell, M. J.; Kochanek, P. M.; Doughty, L. A.; Carrillo, J. A.; Adelson, P. D.; Clark, R. S. B.; Wisniewski, S. R.; Whalen, M.; DeKosky, S. T. Interleukin-6 and Interleukin-10 in Cerebrospinal Fluid after Severe Traumatic Brain Injury in Children. *J. Neurotrauma* **1997**, *14* (7), 451–457.
- (20) Maier, B.; Schwerdtfeger, K.; Mautes, A.; Holanda, M.; Müller, M.; Steudel, W. I.; Marzi, I. Differential Release of Interleukines 6, 8, and 10 in Cerebrospinal Fluid and Plasma after Traumatic Brain Injury. *Shock* **2001**, *15*, 421–426.
- (21) Csuka, E.; Morganti-Kossmann, M. C.; Lenzlinger, P. M.; Joller, H.; Trentz, O.; Kossmann, T. IL-10 Levels in Cerebrospinal Fluid and Serum of Patients with Severe Traumatic Brain Injury: Relationship to IL-6, TNF-Alpha, TGF-Beta1 and Blood-Brain Barrier Function. *J. Neuroimmunol.* **1999**, *101* (2), 211–221.
- (22) Shatara, F. I. Lumbar Puncture in Head Injuries. *Am. J. Surg.* **1936**, *33* (2), 204–209.
- (23) Bauer, M.; Sohm, F.; Thomé, C.; Ortler, M. Refractory Intracranial Hypertension in Traumatic Brain Injury: Proposal for a Novel Score to Assess the Safety of Lumbar Cerebrospinal Fluid Drainage. *Surg. Neurol. Int.* **2017**, *8*, 265.
- (24) Pui, T. S.; Kongsuphol, P.; Arya, S. K.; Bansal, T. Detection of Tumor Necrosis Factor (TNF-Alpha) in Cell Culture Medium with Label Free Electrochemical Impedance Spectroscopy. *Sens. Actuators, B* **2013**, *181*, 494–500.
- (25) Arya, S. K.; Estrela, P. Electrochemical Immunosensor for Tumor Necrosis Factor-Alpha Detection in Undiluted Serum. *Methods* **2017**, *116*, 125–131.
- (26) Jiang, C.; Alam, M. T.; Silva, S. M.; Taufik, S.; Fan, S.; Gooding, J. J. Unique Sensing Interface That Allows the Development of an Electrochemical Immunosensor for the Detection of Tumor Necrosis Factor α in Whole Blood. *ACS Sens.* **2016**, *1* (12), 1432–1438.
- (27) Melow, S. L.; Miller, D. R.; Gizzie, E. A.; Cliffel, D. E. A Low-Interference, High-Resolution Multianalyte Electrochemical Biosensor. *Anal. Methods* **2020**, *12* (31), 3873–3882.
- (28) Angus, D. C.; Linde-Zwirble, W. T.; Lidicker, J.; Clermont, G.; Carcillo, J.; Pinsky, M. R. Epidemiology of Severe Sepsis in the United States: Analysis of Incidence, Outcome, and Associated Costs of Care. *Crit. Care Med.* **2001**, *29* (7), 1303–1310.
- (29) Sands, K. E.; Bates, D. W.; Lanken, P. N.; Graman, P. S.; Hibberd, P. L.; Kahn, K. L.; Parsonnet, J.; Panzer, R.; Orav, E. J.; Snyderman, D. R.; Black, E.; Schwartz, J. S.; Moore, R.; Johnson Jr, B. L.; Platt, R. Epidemiology of Sepsis Syndrome in 8 Academic Medical Centers. *JAMA* **1997**, *278* (3), 234–240.
- (30) Brun-Buisson, C.; Doyon, F.; Carlet, J.; Dellamonica, P.; Gouin, F.; Lepoutre, A.; Mercier, J.-C.; Offenstadt, G.; Régnier, B. Incidence, Risk Factors, and Outcome of Severe Sepsis and Septic Shock in Adults: A Multicenter Prospective Study in Intensive Care Units. *JAMA* **1995**, *274* (12), 968–974.
- (31) Burki, T. K. Sharp Rise in Sepsis Deaths in the UK. *Lancet Respir. Med.* **2018**, *6* (11), 826.
- (32) Molano Franco, D.; Arevalo-Rodriguez, I.; Roqué i Figuls, M.; Montero Oleas, N. G.; Nuvials, X.; Zamora, J. Plasma Interleukin-6 Concentration for the Diagnosis of Sepsis in Critically Ill Adults. *Cochrane Database Syst. Rev.* **2019**, *4* (4), CD011811.
- (33) Leal, Y. A.; Álvarez-Nemegyei, J.; Lavadores-May, A. I.; Girón-Carrillo, J. L.; Cedillo-Rivera, R.; Velazquez, J. R. Cytokine Profile as Diagnostic and Prognostic Factor in Neonatal Sepsis. *J. Matern.-Fetal Neonat. Med.* **2019**, *32* (17), 2830–2836.
- (34) Angurana, S. K.; Bansal, A.; Muralidharan, J.; Aggarwal, R.; Singhi, S. Cytokine Levels in Critically Ill Children With Severe Sepsis and Their Relation With the Severity of Illness and Mortality. *J. Intensive Care Med.* **2021**, *36*, 576.
- (35) Song, J.; Park, D. W.; Moon, S.; Cho, H.-J.; Park, J. H.; Seok, H.; Choi, W. S. Diagnostic and Prognostic Value of Interleukin-6, Pentraxin 3, and Procalcitonin Levels among Sepsis and Septic Shock Patients: A Prospective Controlled Study According to the Sepsis-3 Definitions. *BMC Infect. Dis.* **2019**, *19* (1), 968.
- (36) Miguel-Bayarri, V.; Casanoves-Laparra, E. B.; Pallás-Beneyto, L.; Sancho-Chinesta, S.; Martín-Osorio, L. F.; Tormo-Calandín, C.; Bautista-Rentero, D. Prognostic Value of the Biomarkers Procalcito-

nin, Interleukin-6 and C-Reactive Protein in Severe Sepsis. *Med. Intensiva (English Ed.)* **2012**, *36* (8), 556–562.

(37) Yan, Q.; Zheng, H.-N.; Jiang, C.; Li, K.; Xiao, S.-J. EDC/NHS Activation Mechanism of Polymethacrylic Acid: Anhydride versus NHS-Ester. *RSC Adv.* **2015**, *5* (86), 69939–69947.

(38) Lisdat, F.; Schäfer, D. The Use of Electrochemical Impedance Spectroscopy for Biosensing. *Anal. Bioanal. Chem.* **2008**, *391* (5), 1555–1567.

(39) Russell, C.; Ward, A. C.; Vezza, V.; Hoskisson, P.; Alcorn, D.; Steenson, D. P.; Corrigan, D. K. Development of a Needle Shaped Microelectrode for Electrochemical Detection of the Sepsis Biomarker Interleukin-6 (IL-6) in Real Time. *Biosens. Bioelectron.* **2019**, *126*, 806–814.

(40) Manzanares-Palenzuela, C. L.; Fernandes, E. G. R.; Lobo-Castañón, M. J.; López-Ruiz, B.; Zucolotto, V. Impedance Sensing of DNA Hybridization onto Nanostructured Phthalocyanine-Modified Electrodes. *Electrochim. Acta* **2016**, *221*, 86–95.

(41) Prasad, S.; Selvam, A. P.; Reddy, R. K.; Love, A. Silicon Nanosensor for Diagnosis of Cardiovascular Proteomic Markers. *J. Lab. Autom.* **2013**, *18* (2), 143–151.

(42) Jolly, P.; Formisano, N.; Tkáč, J.; Kasák, P.; Frost, C. G.; Estrela, P. Label-Free Impedimetric Aptasensor with Antifouling Surface Chemistry: A Prostate Specific Antigen Case Study. *Sens. Actuators, B* **2015**, *209*, 306–312.

(43) Bonanni, A.; Pumera, M. Graphene Platform for Hairpin-DNA-Based Impedimetric Genosensing. *ACS Nano* **2011**, *5* (3), 2356–2361.

(44) Lien, T. T. N.; Lam, T. D.; An, V. T. H.; Hoang, T. V.; Quang, D. T.; Khieu, D. Q.; Tsukahara, T.; Lee, Y. H.; Kim, J. S. Multi-Wall Carbon Nanotubes (MWCNTs)-Doped Polypyrrole DNA Biosensor for Label-Free Detection of Genetically Modified Organisms by QCM and EIS. *Talanta* **2010**, *80* (3), 1164–1169.

(45) Centers for Disease Control and Prevention. *Sepsis: Clinical Information*. <https://www.cdc.gov/sepsis/datareports/index.html> (accessed 2021-05-09).

(46) Marik, P. E. Don't Miss the Diagnosis of Sepsis! *Crit. Care* **2014**, *18* (5), 12–14.

(47) Ye, Q.; Wang, B.; Mao, J. The Pathogenesis and Treatment of the “Cytokine Storm” in COVID-19. *J. Infect.* **2020**, *80* (6), 607–613.

(48) Coomes, E. A.; Haghbayan, H. Interleukin-6 in COVID-19: A Systematic Review and Meta-Analysis. *Rev. Med. Virol.* **2020**, *30* (6), 1–9.

(49) Herold, T.; Jurinovic, V.; Arnreich, C.; Lipworth, B. J.; Hellmuth, J. C.; von Bergwelt-Baildon, M.; Klein, M.; Weinberger, T. Elevated Levels of IL-6 and CRP Predict the Need for Mechanical Ventilation in COVID-19. *J. Allergy Clin. Immunol.* **2020**, *146* (1), 128–136.

(50) Gong, J.; Dong, H.; Xia, Q.; Huang, Z.; Wang, D.; Zhao, Y.; Liu, W.; Tu, S.; Zhang, M.; Wang, Q.; Lu, F. Correlation Analysis between Disease Severity and Inflammation-Related Parameters in Patients with COVID-19: A Retrospective Study. *BMC Infect. Dis.* **2020**, *20* (1), 963.